The Astrophysical Journal, 784:78 (8pp), 2014 March 20 doi:10.1088/0004-637X/784/1/78

MASSIVE MOLECULAR GAS FLOWS IN THE A1664 BRIGHTEST CLUSTER GALAXY

H. R. Russell[1], B. R. McNamara[1,2,3], A. C. Edge[4], P. E. J. Nulsen[3], R. A. Main[1], A. N. Vantyghem[1], F. Combes[5], A. C. Fabian[6], N. Murray[7], P. Salomé[5], R. J. Wilman[4], S. A. Baum[8], M. Donahue[9], C. P. O'Dea[8], J. B. R. Oonk[10], G. R. Tremblay[11], and G. M. Voit[9]

[1] Department of Physics and Astronomy, University of Waterloo, Waterloo, ON N2L 3G1, Canada
[2] Perimeter Institute for Theoretical Physics, Waterloo, Canada
[3] Harvard-Smithsonian Center for Astrophysics, 60 Garden Street, Cambridge, MA 02138, USA
[4] Department of Physics, Durham University, Durham DH1 3LE, UK
[5] L'Observatoire de Paris, 61 Av. de L'Observatoire, F-75 014 Paris, France
[6] Institute of Astronomy, Madingley Road, Cambridge, CB3 0HA, UK
[7] Canadian Institute for Theoretical Astrophysics, University of Toronto, 60 St. George Street, Toronto, M5S 3H8 Ontario, Canada
[8] School of Physics and Astronomy, Rochester Institute of Technology, Rochester, NY 14623, USA
[9] Department of Physics and Astronomy, Michigan State University, 567 Wilson Road, East Lansing, MI 48824, USA
[10] Netherlands Institute for Radio Astronomy, Postbus 2, 7990 AA Dwingeloo, The Netherlands
[11] European Southern Observatory, Karl-Schwarzschild-Strasse 2, D-85748 Garching, Germany
Received 2013 August 28; accepted 2014 January 14; published 2014 March 6

ABSTRACT

We report ALMA Early Science CO(1–0) and CO(3–2) observations of the brightest cluster galaxy (BCG) in A1664. The BCG contains $1.1 \times 10^{10}\,M_{\odot}$ of molecular gas divided roughly equally between two distinct velocity systems: one from −250 to +250 km s^{-1} centered on the BCG's systemic velocity and a high-velocity system blueshifted by 570 km s^{-1} with respect to the systemic velocity. The BCG's systemic component shows a smooth velocity gradient across the BCG center, suggestive of rotation about the nucleus. However, the mass and velocity structure are highly asymmetric and there is little star formation coincident with a putative disk. It may be an inflow of gas that will settle into a disk over several 10^8 yr. The high-velocity system consists of two gas clumps, each ∼2 kpc across, located to the north and southeast of the nucleus. Each has a line of sight velocity spread of 250–300 km s^{-1}. The velocity of the gas in the high-velocity system increases toward the BCG center and may be a massive flow into the nucleus. However, the velocity gradient is not smooth. These structures are also coincident with low optical–ultraviolet surface brightness regions, which could indicate dust extinction associated with each clump. The structure is complex, making a clear interpretation difficult, but if the dusty, molecular gas lies predominantly in front of the BCG, the blueshifted velocities would indicate an outflow. Based on the energy requirements, such a massive outflow would most likely be driven by the active galactic nucleus. A merger origin is unlikely but cannot be ruled out.

Key words: galaxies: active – galaxies: clusters: individual (A1664) – galaxies: ISM – galaxies: kinematics and dynamics

Online-only material: color figures

1. INTRODUCTION

Containing molecular gas reservoirs upward of $10^9\,M_{\odot}$ and in some cases approaching $10^{11}\,M_{\odot}$, brightest cluster galaxies (BCGs) are among the most molecular gas-rich early-type galaxies in the nearby universe (Donahue et al. 2000; Edge 2001; Edge & Frayer 2003; Salomé & Combes 2003). BCGs with large quantities of cool gas reside almost exclusively at the centers of clusters whose hot atmospheres have short central radiative cooling times (<1 Gyr; Heckman 1981; Cowie et al. 1983; Hu et al. 1985). In addition to molecular gas, these BCGs are forming stars at rates of several to tens of solar masses per year (e.g., Johnstone et al. 1987; O'Dea et al. 2008). The origin of this gas has been attributed to either gas-rich mergers or cooling from the hot atmospheres surrounding the BCG. However, several lines of evidence strongly suggest that the molecular gas cooled from the hot atmosphere and accreted onto the BCG, fueling star formation. Although BCGs harbor substantial amounts of molecular gas and star formation, this is typically only a small fraction of the material that is expected to cool out of the hot atmosphere over time (e.g., Fabian 1994; Edge 2001; Salomé & Combes 2003).

It is now believed that radiative cooling is regulated by feedback from the active galactic nucleus (AGN; e.g., Peterson & Fabian 2006; McNamara & Nulsen 2007). This so-called radio-mode feedback is thought to operate primarily on the hot volume-filling atmosphere, which prevents or regulates the rate of cooling onto the BCG and in turn the level of fueling onto the supermassive black hole. However, the degree to which radio-mode feedback also operates on the cold molecular gas is unclear. Early indications that radio jets interact with the cold atomic gas have been found in observations of ionized gas in powerful radio galaxies (e.g., Tadhunter 1991; Veilleux et al. 2002; Emonts et al. 2005; Nesvadba et al. 2006) and H I absorption, which show high-speed outflows of neutral hydrogen (e.g., Morganti et al. 1998; Oosterloo et al. 2000; Morganti et al. 2004, 2005). However, without accurate outflow mass estimates, it is difficult to evaluate their impact on the evolution of galaxies.

Cycle 0 ALMA observations of the A1835 BCG reveal an apparent outflow of molecular gas with a mass exceeding $10^{10}\,M_{\odot}$. Its close association with the X-ray cavities and the inability of the radiation and mechanical energy from supernovae to drive such a massive flow of gas suggests that the radio AGN is powering the outflow (McNamara et al. 2013). These results imply

that radio-mode feedback couples not only to volume-filling hot atmospheres, but is able to drive outward the high-density molecular gas in galaxies. Here, we present new ALMA Early Science observations of the BCG in A1664 and report the discovery of massive flows of molecular gas in the BCG. We assume $H_0 = 70\,\mathrm{km\ s^{-1}\ Mpc^{-1}}$, $\Omega_m = 0.3$, and $\Omega_\Lambda = 0.7$. For this cosmology, 1″ corresponds to a physical scale of 2.3 kpc at the redshift $z = 0.128$ of the BCG (Allen et al. 1992; Pimbblet et al. 2006). This redshift is based predominantly on emission-line observations and is accurate to roughly $100\,\mathrm{km\ s^{-1}}$. All errors are 1σ unless otherwise noted.

2. DATA REDUCTION

The BCG in A1664 was observed with the band 3 and the band 7 receivers on ALMA as a Cycle 0 Early Science program (ID = 2011.0.00374.S; PI McNamara). These data were obtained in two 25 minute observations in band 3 on 2012 March 27 and April 7 and in two 35 minute observations in band 7 on 2012 March 28. On average, sixteen 12 m antennas were used in the extended configuration with baselines up to 400 m. The observations used a single pointing centered on the BCG in A1664. The receiver was tuned to cover the redshifted ^{12}CO(1–0) line at 102.2 GHz in the band 3 upper sideband and the ^{12}CO(3–2) line at 306.7 GHz in the band 7 upper sideband. Each spectral window had a bandwidth of 1.875 GHz and two spectral windows were set in each sideband, providing a total frequency range of ∼7 GHz. A spectral resolution of 0.488 MHz per channel was used but channels were binned together to improve the signal-to-noise ratio. The bright quasar 3C 279 was observed for bandpass calibration and observations of Mars provided absolute flux calibration. Observations switched from A1664 to the nearby phase calibrator J1246−257 every ∼10 minutes.

The observations were calibrated using the CASA software (version 3.3; McMullin et al. 2007), following the detailed processing scripts provided by the ALMA science support team. The continuum-subtracted images were reconstructed using the CASA task CLEAN assuming Briggs weighting with a robustness parameter of 0.5 and a simple polygon mask applied to each channel. This provided a synthesized beam of $1\farcs4 \times 1\farcs1$ with a position angle (P.A.) of $-79\fdg1$ at CO(1–0) and $0\farcs55 \times 0\farcs39$ with a P.A. $-81\fdg4$ at CO(3–2). The rms noise in the line-free channels was $0.5\,\mathrm{mJy\ beam^{-1}}$ for $40\,\mathrm{km\ s^{-1}}$ channels at CO(1–0) and $1.5\,\mathrm{mJy\ beam^{-1}}$ for $30\,\mathrm{km\ s^{-1}}$ channels at CO(3–2). Images of the continuum emission were also produced with CLEAN by averaging channels free of any line emission. A central continuum source is detected in both bands, possibly partially resolved in band 7, with flux 2.5 ± 0.2 mJy in band 3 and 1.1 ± 0.1 mJy in band 7. The mm-continuum source position coincides with the Very Large Array radio nucleus position (M. T. Hogan et al., in preparation). The mm-continuum flux is also consistent, within a factor of two, with synchrotron emission from a flat spectrum radio core[12] with $\alpha \approx 0.5$ (Hogan et al., in preparation), suggesting this is the location of the low-luminosity AGN.

3. RESULTS

3.1. Spectra and Integrated Intensity Maps

We detected and imaged both CO(1–0) and CO(3–2) rotational transition lines in the BCG of A1664. Figure 1 shows the continuum-subtracted total spectral line profiles extracted from a $6'' \times 6''$ region at CO(1–0) and a $3'' \times 3''$ region at CO(3–2). A larger $6'' \times 6''$ region at CO(3–2) produces a consistent total flux but a significantly noisier spectrum. Both the CO(1–0) and CO(3–2) line profiles show two distinct components: a broad component centered on the BCG's systemic velocity and a narrower high-velocity system (HVS) blueshifted to $-570\,\mathrm{km\ s^{-1}}$. These spectral profiles were each fit with two Gaussian components using the package MPFIT (Markwardt 2009) and the best-fit results are shown in Table 1. Although the BCG's systemic component is significantly broader, the peak flux for the HVS is roughly a factor of two higher, producing a similar integrated intensity for each component. The total CO(1–0) integrated intensity of $3.2 \pm 0.4\,\mathrm{Jy\ km\ s^{-1}}$ is roughly half of the IRAM single-dish signal found by Edge (2001). This may be due to uncertainties in the continuum baseline subtraction or may indicate more extended emission filtered out by the interferometer or lying below our sensitivity. Missing short spacings will filter out extended emission at scales larger than ∼9″ at CO(1–0) and ∼3″ at CO(3–2).

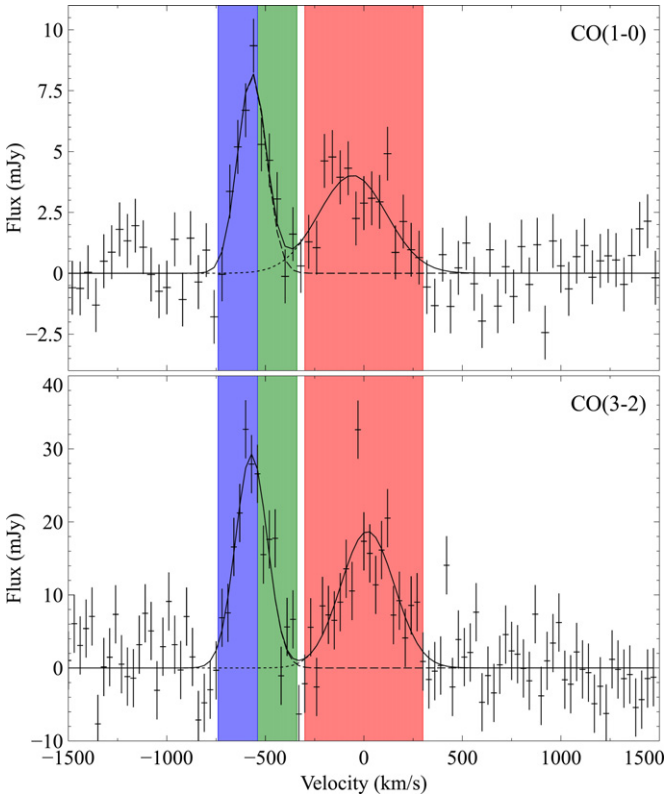

Figure 1. A1664 CO(1–0) (top) and CO(3–2) (bottom) total spectra for $6'' \times 6''$ and $3'' \times 3''$ regions, respectively. A larger $6'' \times 6''$ region at CO(3–2) produces a consistent total flux but a significantly noisier spectrum. Two-component model fits shown by a solid line with individual Gaussians shown by dashed and dotted lines. The colored velocity bands correspond to the velocity ranges of the image contours in Figures 2 and 3.

(A color version of this figure is available in the online journal.)

Integrated intensity maps of the CO(1–0) and CO(3–2) emission are displayed in Figures 2 and 3 with no threshold value adopted on the intensities. This combination gives a higher resolution image of the molecular gas near the nucleus at CO(3–2) and sensitivity over more extended scales at CO(1–0). The bulk of the molecular gas is concentrated in the galaxy center within a ∼3″ radius at CO(1–0) and a ∼1.5″ radius at CO(3–2). We have produced contours from integrated intensity

[12] For the convention $f_\nu \propto \nu^{-\alpha}$.

Table 1
Fit Parameters for the Total Emission line Spectrum at CO(1–0) and CO(3–2)

CO Line	ν_{rest} (GHz)	ν_{obs} (GHz)	χ^2/dof	Gaussian Component	Integrated Intensity[a] (Jy km s^{-1})	Peak (mJy)	FWHM[b] (km s^{-1})	Velocity Shift (km s^{-1})	Mass[c] (10^9 $M_\odot$)
$J = 1$–0	115.27	102.19	100/94	1	1.5 ± 0.2	8.2 ± 0.8	170 ± 20	-568 ± 8	5.0 ± 0.7
				2	1.7 ± 0.3	4.0 ± 0.5	400 ± 60	-60 ± 20	5.7 ± 1.0
$J = 3$–2	345.80	306.56	126/94	1	5.9 ± 0.7	29 ± 2	190 ± 20	-571 ± 7	
				2	6.4 ± 0.9	19 ± 2	320 ± 30	20 ± 10	

Notes.
[a] The integrated line intensities have been corrected for the primary beam response.
[b] The line widths have been corrected for instrumental broadening.
[c] The molecular gas mass was calculated from the CO(1–0) integrated intensity, as described in Section 4.1.

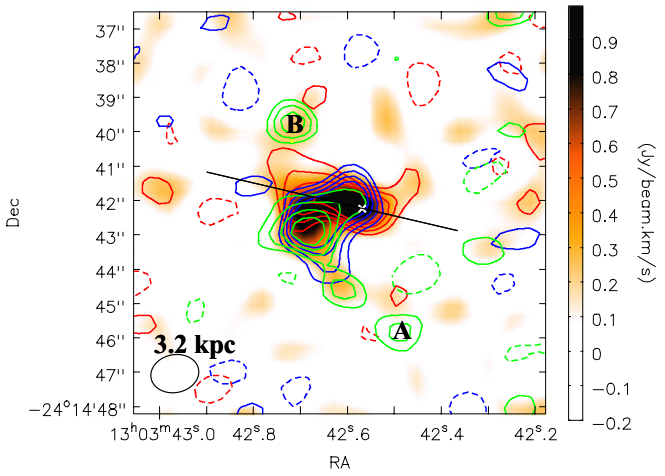

Figure 2. A1664 CO(1–0) integrated intensity map for velocities −740 to 300 km s^{-1} with contours for the disk component (−300 to 300 km s^{-1}, red) and the HVS (−740 to −540 km s^{-1}, blue and −540 to −340 km s^{-1}, green). The contours are -2σ, 2σ, 3σ, 4σ, and 5σ, where $\sigma = 0.084$ Jy beam^{-1} km s^{-1} (red), 0.047 Jy beam^{-1} km s^{-1} (blue), and 0.046 Jy beam^{-1} km s^{-1} (green). The continuum nucleus is marked by a cross and the ALMA beam size is shown in the lower left. The black line shows the axis of the position–velocity diagram in Figure 4. The image has not been corrected for the primary beam.
(A color version of this figure is available in the online journal.)

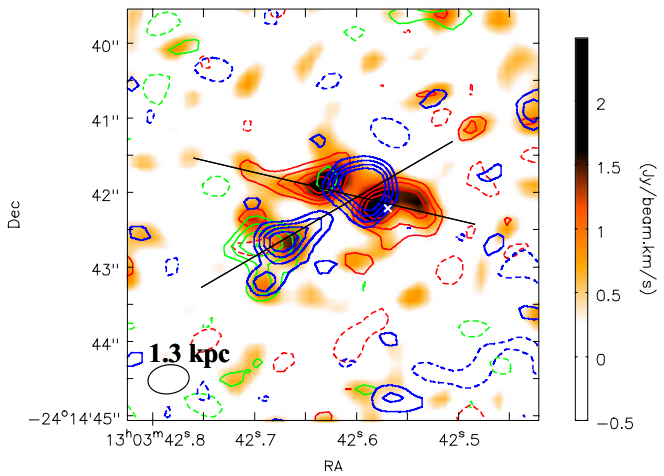

Figure 3. A1664 CO(3–2) integrated intensity map for velocities −735 to 285 km s^{-1}, with contours for the disk component (−285 to 285 km s^{-1}, red) and the HVS (−735 to −525 km s^{-1}, blue and −525 to −345 km s^{-1}, green). The contours are -2σ, 2σ, 3σ, 4σ, and 5σ, where $\sigma = 0.25$ Jy beam^{-1} km s^{-1} (red), 0.15 Jy beam^{-1} km s^{-1} (blue), and 0.13 Jy beam^{-1} km s^{-1} (green). Negative contours are shown by a dashed line. The continuum nucleus is marked by a cross and the ALMA beam size is shown in the lower left. The black lines show the axes of the position–velocity diagrams in Figures 4 and 5. The image has not been corrected for the primary beam.
(A color version of this figure is available in the online journal.)

maps covering the velocity range of the BCG's systemic component (red) and the HVS (blue and green) to show their spatial extent. Both maps show a similar morphology with these two components separated spatially as well as spectrally. The kinematics of these two components broadly match those found in Hα, Paα, and ro-vibrational H_2 integral field unit (IFU) observations of the BCG (Wilman et al. 2006, 2009).

In CO(1–0), the BCG's systemic component extends ∼5″ (11 kpc) from northeast to southwest, covering a velocity range from −250 km s^{-1} to +250 km s^{-1} and roughly peaking on the continuum position. The line emission from this component is highly asymmetric about the nucleus with the greatest extent toward the northeast. There is approximately twice as much CO(1–0) flux to the northeast of the nucleus compared with the southwest.

The HVS extends ∼4″ (9 kpc) from northwest to southeast and covers a velocity range from −700 to −450 km s^{-1}. It appears marginally to the north and east of the nucleus and, given the uncertainty in its position along the line of sight through the galaxy, it is not clear if the HVS physically interacts with the BCG's systemic component.

The CO(3–2) map shows a morphology broadly similar to the CO(1–0) but reveals more complex structure on smaller scales. There is an apparent drop in the intensity of the BCG's systemic component where it overlaps with the HVS, possibly suggesting a physical interaction between these components. The southwest blob of the BCG's systemic component is roughly spatially coincident with the AGN. The HVS may separate into two gas blobs, each contained within a projected diameter of ∼2 kpc. One clump is projected immediately to the north of the nucleus, where the deficit of emission is seen in the BCG's systemic component. The second high-velocity clump appears ∼3 kpc in projection to the southest and extends toward the northern clump. It could be one extended filament.

In Figures 2 and 3, the HVS has been subdivided into higher (blue) and lower (green) velocity contours to show that the lower velocity gas in this component tends to lie at larger distances from the nucleus. There is a shift in the velocity of the gas in the HVS at CO(3–2) from -510 ± 20 km s^{-1} in the southeast blob to -590 ± 10 km s^{-1} in the northern clump. The FWHM of the HVS at CO(3–2) is $\sim 230 \pm 30$ km s^{-1} in the southeast blob but drops to 130 ± 10 km s^{-1} in the clump to the north

of the nucleus. Although the separate clumps of the HVS are spatially unresolved at CO(1–0), there is a shift in the velocity from -545 ± 9 km s^{-1} to -600 ± 10 km s^{-1} along the HVS filament toward the nucleus and a corresponding decrease in the FWHM from 200 ± 20 km s^{-1} to 130 ± 30 km s^{-1}, consistent with the CO(3–2) results.

The gas clumps labeled A and B in Figure 2 appear to be separate structures with velocities of -400 ± 20 km s^{-1} and -370 ± 40 km s^{-1}, respectively. Using a single Gaussian component fit to each spectrum, the integrated intensity was 0.17 ± 0.07 Jy km s^{-1} for gas clump A and 0.3 ± 0.1 Jy km s^{-1} for gas clump B. Gas clump A is also observed at CO(3–2) with an integrated intensity of 0.8 ± 0.2 Jy km s^{-1} but gas clump B is not detected.

3.2. Position–Velocity Diagrams

Figure 4 shows the position–velocity (PV) cuts along P.A. = 77° (defined east from north) across the BCG's systemic component from northeast to southwest at CO(1–0) and CO(3–2). A two-dimensional Gaussian was fit to the integrated intensity maps of the BCG systemic component to determine this best-fit P.A. and this was found to be consistent at both CO(1–0) and CO(3–2) within the error. The PV slices summed the line emission across the width of the BCG's systemic component. The CO(1–0) PV diagram shows a smooth velocity gradient from -250 km s^{-1} to +250 km s^{-1}, with no visible flattening of the gradient at large radii. The CO(3–2) emission also traces this steady velocity gradient. This appears consistent with a flattened disk-like structure rotating in the rest frame of the BCG but the radial velocity profile is not clear. The velocity structure is similar to that of the rotating gas disk in Hydra A (e.g., Simkin 1979; Ekers & Simkin 1983; Wilman et al. 2005; Hamer et al. 2013). The AGN appears offset from the gas dynamical center by $\sim 0.5''$ but this may instead be due to the uncertainty in the systemic velocity. The emission is clumpy and strongly asymmetric about the nucleus at both CO(1–0) and CO(3–2), suggesting the disk may be only partially filled (e.g., Wilman et al. 2005).

Figure 5 shows a PV slice along the HVS from southeast to northwest with a best-fit P.A. = 120° at CO(3–2). The HVS may separate into two gas blobs, each with a very broad velocity dispersion of close to 300 km s^{-1}. The velocity at the peak intensity shifts from ~ -450 km s^{-1} to ~ -600 km s^{-1} from the southeast to the northwest blob but there is not a clear velocity gradient for the intervening gas, as found for the BCG's systemic component. The PV diagram for the HVS at CO(1–0) shows a similar velocity structure but at lower spatial resolution.

4. DISCUSSION

Our CO(1–0) and CO(3–2) observations show that the BCG in A1664 harbors two large gas flows projected across the galaxy center at velocities from -700 to -450 km s^{-1} and -250 to +250 km s^{-1}. These molecular gas structures and their kinematics match those found in IFU observations of the BCG covering Hα, Paα, and rovibrational H_2 (Wilman et al. 2006, 2009). In the following, we calculate the molecular gas masses of these flows and consider their possible origins including mergers, inflow settling into a disk, and outflow.

4.1. Molecular Gas Mass

From the integrated CO(1–0) intensities, $S_{\rm CO}\Delta v$, in Table 1, we calculated the molecular gas mass:

$$M_{\rm mol} = 1.05 \times 10^4 X_{\rm CO} \left(\frac{1}{1+z}\right) \left(\frac{S_{\rm CO}\Delta v}{\rm Jy\ km\ s^{-1}}\right) \left(\frac{D_{\rm L}}{\rm Mpc}\right)^2 M_\odot, \quad (1)$$

where $X_{\rm CO}$ is the CO-to-H_2 conversion factor ($\rm cm^{-2}\,(K\,km\,s^{-1})^{-1}$), $D_{\rm L}$ is the luminosity distance, and z is the BCG redshift (e.g., Solomon et al. 1987; Solomon & Vanden Bout 2005; Bolatto et al. 2013). Under the assumption of the Galactic value $X_{\rm CO} = 2 \times 10^{20}$ $\rm cm^{-2}\,(K\,km\,s^{-1})^{-1}$, we find a molecular gas mass for the BCG's systemic component of $M_{\rm disk} = (5.7 \pm 1.0) \times 10^9\ M_\odot$ and a mass for the HVS of $M_{\rm HVS} = (5.0 \pm 0.7) \times 10^9\ M_\odot$. The total molecular gas mass in the BCG is then $(1.1 \pm 0.1) \times 10^{10}\ M_\odot$. The two separate gas clumps, A and B (Figure 2), have molecular gas masses of $(6 \pm 2) \times 10^8\ M_\odot$ and $(1.0 \pm 0.3) \times 10^9\ M_\odot$, respectively. The true value of $X_{\rm CO}$ may depend on environmental factors such as the gas phase metal abundance, temperature, density, and dynamics.

The central gas surface density of $\sim 200\ M_\odot$ pc^{-2} is not unusual for a star-forming disk (e.g., Bolatto et al. 2013). The star-forming regions produce U-band continuum emission from which Kirkpatrick et al. (2009) determine a star formation rate of $\sim 20\ M_\odot$ yr^{-1}. There is no bright point source associated with the AGN. For a radius of ~ 3 kpc, the surface densities of star formation and molecular gas are $\log\Sigma_{\rm SFR} = -0.2\ M_\odot$ yr^{-1} kpc^{-2} and $\log\mu_{\rm CO} = 2.3\ M_\odot$ pc^{-2}, respectively. The A1664 BCG lies with circumnuclear starbursts and central regions of normal disks on the Schmidt–Kennicutt relation (Kennicutt 1998), showing that despite the massive gas flows it is similar to other normal galaxies. The surrounding X-ray atmosphere, from which the molecular gas presumably cooled, also has a subsolar metallicity (0.5–1 $Z_\odot$, Kirkpatrick et al. 2009). Therefore, we argue that the Galactic $X_{\rm CO}$ value is likely to be reasonable. Even if $X_{\rm CO}$ lies a factor of a few below the Galactic value, the molecular gas flows reported here would still exceed $10^9\ M_\odot$, which would not qualitatively alter our conclusions (e.g., McNamara et al. 2013).

4.2. Mergers

Kirkpatrick et al. (2009) noted that at least four galaxies are projected against the envelope of the BCG, raising the possibility of a merger. Although no galaxy is observed coincident with the HVS, the central optical morphology is complicated by bright knots of star formation and dust regions (Figure 6; O'Dea et al. 2010). It is therefore difficult to rule out a collision but there are several factors weighing against this hypothesis. The BCG resides at the center of a dense cluster atmosphere. A galaxy plunging into the center would likely be stripped of most of its gas before it reached the BCG (e.g., Vollmer et al. 2008; Kirkpatrick et al. 2009; Jablonka et al. 2013). Although molecular gas is more resilient to ram pressure stripping than atomic gas, the molecular gas masses in the BCG and the HVS are unusually large and there are few galaxies in nearby clusters harboring this much gas (e.g., Combes et al. 2007; Young et al. 2011). In the context of a merger scenario, the different velocities of the BCG's systemic component and the HVS may require two unlikely merger events. These interactions would also have to be close to direct hits to the BCG center, which again would be unlikely (e.g., Benson 2005).

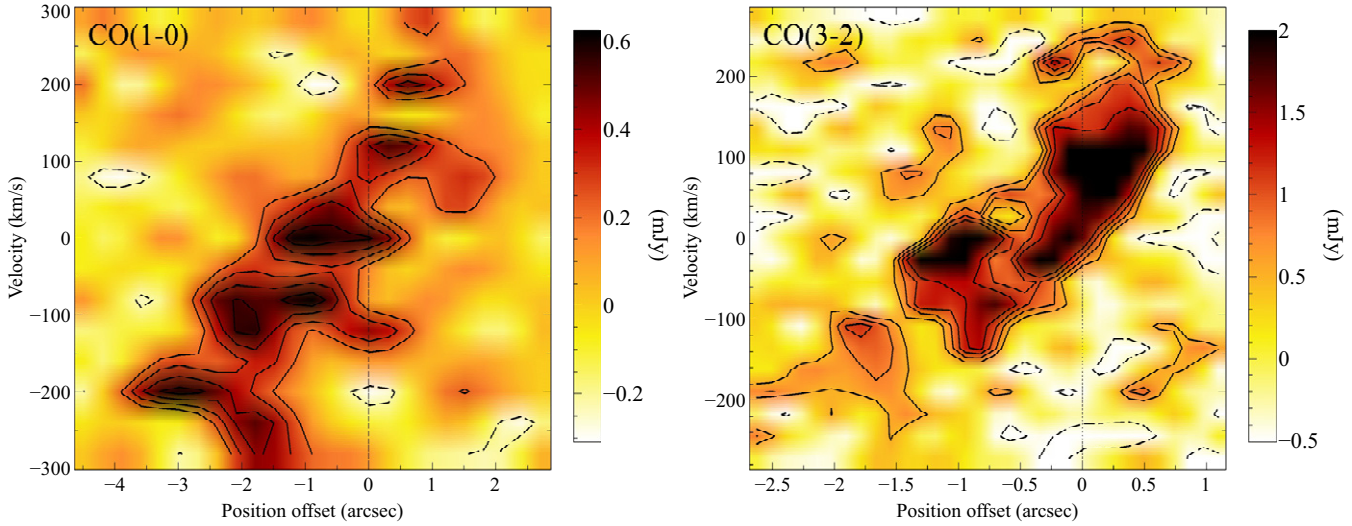

Figure 4. Position–velocity diagrams for the BCG's systemic component at CO(1–0) (left) and CO(3–2) (right), each taken through a slice with P.A. = 77°. The molecular gas in this structure extends from the northeast, at velocities of −250 km s^{-1}, to the southwest, at velocities of +250 km s^{-1}. The contours are -2σ, 2σ, 3σ, 4σ, and 5σ. Negative contours are shown by a dashed line. The dotted straight line marks the continuum point source position.

(A color version of this figure is available in the online journal.)

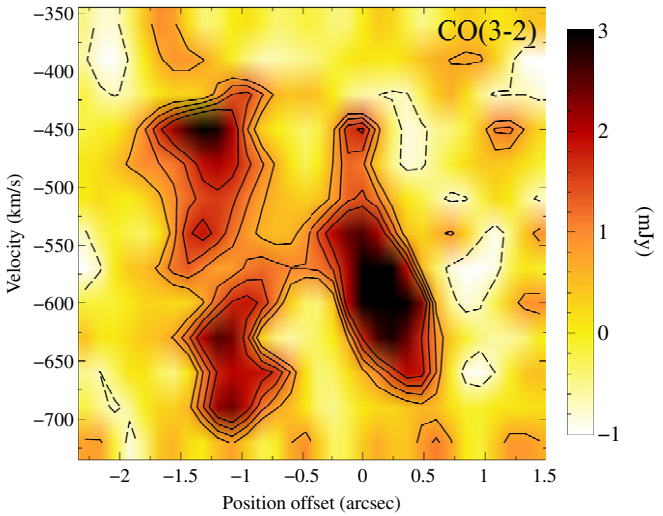

Figure 5. A1664 CO(3–2) position–velocity diagram for the HVS taken through a slice with P.A. = 120°. The slice runs from the southeast to the northwest and is centered on the point where the HVS intersects the BCG's systemic component (see Figure 3). The contours are -2σ, 2σ, 3σ, 4σ, and 5σ. Negative contours are shown by a dashed line.

(A color version of this figure is available in the online journal.)

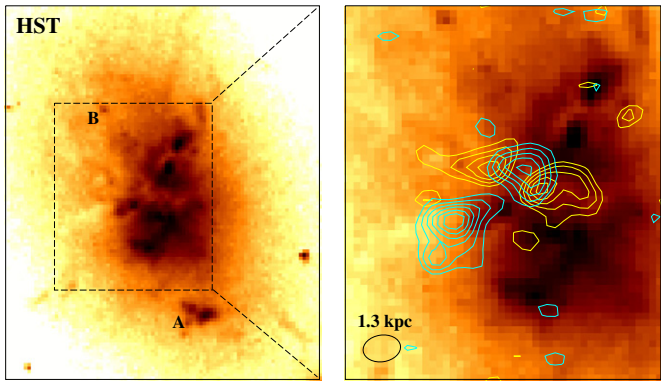

Figure 6. Left: *Hubble Space Telescope (HST)* WFPC2 F606W optical image of the BCG in A1664. Right: zoom-in of the *HST* image with ALMA CO(3–2) contours representing the BCG's systemic component (−285 to 285 km s^{-1}; yellow) and HVS (−705 to −405 km s^{-1}; cyan). The ALMA beam size for CO(3–2) is shown to the lower left.

(A color version of this figure is available in the online journal.)

4.3. Inflow

It is more likely that such large quantities of molecular gas originated in gas cooling from the hot cluster atmosphere (Edge 2001; Salomé & Combes 2003). In BCGs, there are clear associations between the shortest radiative X-ray cooling times, the strength of optical line emission, CO and H_2 emission, and star formation (Cowie et al. 1983; Crawford et al. 1999; Peres et al. 1998; Rafferty et al. 2008). The BCG in A1664 is among the brightest Hα emitters in the Crawford et al. (1999) *ROSAT* brightest cluster sample, the Hα emission aligns with the soft X-ray emission (Allen et al. 1995), and the X-ray radiative cooling time in the center is short (0.4 Gyr; Kirkpatrick et al. 2009). In the nearby BCG NGC 1275, the CO filaments are co-spatial with the coolest X-ray gas and the outer two filaments have radial velocity gradients with larger blueshifted velocities at smaller radii (Salomé et al. 2006; Lim et al. 2008). The molecular gas kinematics are consistent with free fall in the gravitational potential of NGC 1275, as expected if they originated in cooling from the X-ray atmosphere.

For radial inflow, we expect velocity gradients increasing toward the nucleus with the largest velocities toward the BCG center. Although there is not a clear, smooth velocity gradient across the HVS, the lower velocity gas in this component does tend to lie at a greater distance from the nucleus, suggesting an inflow is plausible. The extent and velocity shifts across the HVS gas clumps and the BCG's systemic component can be used to constrain their dynamics and origin (Figure 3). The velocity shear across the gas clumps in the HVS is ∼250–300 km s^{-1} along the line of sight (Figure 5). A similar shear in the transverse direction could have separated the clouds on the observed scale in only $\sim 10^7$ yr. Therefore, the clumps are of order that age or the clouds are moving nearly along the line of sight. In the latter

case, the broad velocity shear could signify a velocity gradient with high-velocity infall onto the nucleus.

The BCG's systemic component has a clear and smooth velocity gradient with a velocity increase of $\sim$500 km s^{-1} over its $\sim$11 kpc length. The velocity profile of this component is suggestive of rotation about the BCG center; however, the mass and velocity structure are strongly asymmetric (Section 3.1). For a putative rotating disk, we estimate the Toomre Q criterion for disk stability (Toomre 1964), $Q = v_c v_T/\pi G r \Sigma$, where the circular velocity is $v_c \sim 200$ km s^{-1}, the turbulent velocity is $v_T \sim$ 50–100 km s^{-1}, the disk radius is $r \sim 3$ kpc, and the disk surface density is $\Sigma \sim 200\ M_\odot$ pc^{-2}. Although highly uncertain, we estimate that the Q parameter is of order one, which is a reasonable value for a normal disk and suggestive that it could be unstable and potentially star forming. However, Figure 6 does not show strong star formation associated with the BCG's systemic component. Star formation could be obscured by dust but the U-band star formation rate, SFR$_U \sim 20\ M_\odot$ yr^{-1} (Kirkpatrick et al. 2009), and the infrared star formation rate, SFR$_{IR} = 15\ M_\odot$ yr^{-1} (O'Dea et al. 2008), are comparable, which is inconsistent with buried star formation. This could be a recent infall of material that is in the process of settling into a disk around the nucleus. Its orbital time is $\sim 9 \times 10^7$ yr so a relaxed disk will take at least several 10^8 yr to form.

An X-ray cooling origin for the gas inflow must explain how molecular hydrogen can form in this environment. It is difficult to form molecular hydrogen rapidly in these systems by a process other than catalytic reactions on dust grain surfaces (e.g., Fabian et al. 1994). Hot ions in the X-ray atmosphere will destroy unshielded dust on much shorter timescales than the radiative cooling time (e.g., Draine & Salpeter 1979). Yet, dust does appear to be a ubiquitous feature of the colder gas phases in these systems (e.g., Egami et al. 2006; Donahue et al. 2007; Quillen et al. 2008; Mittal et al. 2011). Fabian et al. (1994) have speculated that dust may somehow form deep within very cold gas clouds, but ab initio dust formation by coagulation of atoms is likely to be a slow process and difficult in an environment where X-rays can quickly destroy small clusters of atoms (e.g., Voit & Donahue 1995). If dust-rich stellar ejecta from the BCG and ongoing star formation can be mixed into cooling X-ray gas before the dust grains are destroyed by sputtering, then those seed grains may act as sites for further dust nucleation (Voit & Donahue 2011; Panagoulia et al. 2013). Dusty gas clouds could be dragged out from the BCG by buoyantly rising radio bubbles and promote subsequent molecular formation (see Section 4.4.2; e.g., Ferland et al. 2009; Salomé et al. 2011).

4.4. Outflow

Without additional absorption line observations, it is difficult to determine whether the gas flows lie in front or behind the BCG along the line of sight. Therefore, we cannot distinguish between an inflow of gas located behind the BCG and an outflow of gas located in front of the BCG. Figure 6 shows that the molecular gas clumps appear coincident with regions of lower optical–ultraviolet (UV) surface brightness in the BCG, which could indicate either a physical reduction in the emission or dust obscuration. Gas clumps A and B are associated with bright optical–UV knots. The complexity of the structure makes a clear interpretation difficult but it is plausible that the dusty molecular gas lies predominantly in front of the BCG and that the blueshifted velocities indicate an outflow.

4.4.1. Driving an Outflow with Radiation Pressure or Supernovae

Radiation pressure from young stars will drive out the molecular gas if the radiative force exceeds the gravitational force on the cloud, $L_{UV}/c > Mg$. We estimate the gravitational acceleration as $g = 2\sigma^2/R$, where the stellar velocity dispersion for a BCG is typically $\sim$300 km s^{-1} (e.g., von der Linden et al. 2007) and the projected extent of the outflow is $R = 9$ kpc. For an outflow mass $M = 5 \times 10^9\ M_\odot$, this requires a luminosity in excess of 2×10^{46} erg s^{-1}. The far-UV continuum emission from young stars in the A1664 BCG provides $L_{UV} = 1.7 \times 10^{43}$ erg s^{-1} (O'Dea et al. 2010), which is insufficient by three orders of magnitude.

Mechanical winds driven by supernovae can also power molecular gas outflows in galaxies (e.g., Veilleux et al. 2005). Assuming 10^{51} erg per Type II supernova and a supernova production rate of 1 per 127 $M_\odot$ (Hernquist & Springel 2003), the star formation rate in the A1664 BCG of SFR $\sim 20\ M_\odot$ yr^{-1} will generate a mechanical power of $\sim 5 \times 10^{42}$ erg s^{-1}. This falls short of the kinetic power of the outflow, $E_{KE}/t_{out} \sim 2 \times 10^{58}$ erg$/2 \times 10^7$ yr $= 3 \times 10^{43}$ erg s^{-1}, by a factor of $\sim$6 and assumes that all of the mechanical energy is coupled to the gas. Little energy can be radiated. Mechanical winds from supernovae are therefore insufficient to accelerate the molecular gas.

4.4.2. Driving an Outflow with a Radio AGN

Using ALMA Cycle 0 observations of the BCG in A1835, B. R. McNamara et al. (submitted) found a massive $>10^{10}\ M_\odot$ outflow of molecular gas likely driven by the radio AGN. Active central radio sources and radio bubbles inflated by the central AGN are ubiquitous in galaxy clusters with short central cooling times, such as A1664 (Burns 1990; Bîrzan et al. 2004; Dunn & Fabian 2006). The central radio source in the BCG in A1664 is amorphous and fairly weak, similar to A1835. The bulk of the energy from the radio AGN emerges as mechanical energy, which can be estimated using scaling relations between the jet mechanical power and the radio synchrotron power (Bîrzan et al. 2008). Using the 1.4 GHz NVSS and 352 MHz WISH catalog radio fluxes of 36.4 mJy and 329 mJy (Condon et al. 1998; De Breuck et al. 2002), respectively, Kirkpatrick et al. (2009) estimated an AGN mechanical power of ~ 6–8×10^{43} erg s^{-1}. However, this has an order-of-magnitude uncertainty. The outflow velocity of the molecular gas is consistent with the buoyancy speeds of radio bubbles. These are typically a significant fraction of the sound speed in the hot cluster atmosphere (e.g., Bîrzan et al. 2004), which is $\sim$900 km s^{-1} at the center of A1664. For an outflow age of 2×10^7 yr, the energy required to drive a $5 \times 10^9\ M_\odot$ molecular gas outflow at a velocity of 600 km s^{-1} is roughly 35% of the AGN mechanical energy. This is large but plausible given the order-of-magnitude uncertainty on the AGN mechanical power.

Although there is no detection of a counterpart redshifted outflow, the asymmetry may be due to uneven mass loading or a lopsided radio jet in the previous outburst. The molecular gas outflow observed in A1835 (McNamara et al. 2013) is also asymmetric, with a higher mass and broader velocity dispersion observed in the redshifted compared with the blueshifted component.

The putative coupling between the radio outburst and the molecular gas is also not understood. Simulations have shown that ram pressure produced by high Eddington ratio jets is able to couple efficiently to the interstellar medium and drive some of the gas out (e.g., Wagner et al. 2012). However, observations

of A1835 suggest that the molecular gas is being lifted by the updraft in the wake of the radio bubbles (e.g., Pope et al. 2010; McNamara et al. 2013). It is difficult to understand how small and dense molecular gas clouds can be uplifted with entrained hot gas. This could potentially be explained if the molecular gas formed in situ from hotter ∼0.5–1 keV gas rising in the bubbles' wake (e.g., Salomé et al. 2008; Revaz et al. 2008; Salomé et al. 2011). The radiative cooling time of 0.5–1 keV gas in local pressure equilibrium is only a few $\times 10^7$ yr, which is comparable to the rise time of the bubbles and the molecular gas. The 0.5–1 keV gas would have a density only a few times larger than the ambient hot atmosphere but it would be several orders of magnitude less dense than the molecular gas itself, making it much easier to lift and accelerate to the speeds observed. Molecular hydrogen is difficult to form rapidly in these systems without sufficient dust and, if unshielded, dust will be quickly sputtered by the hot X-ray gas (e.g., Draine & Salpeter 1979; Ferland et al. 1994). Dust could, however, be dragged out from the galaxy center by rising bubbles and this may be sufficient for molecular hydrogen formation in extended outflows (e.g., Ferland et al. 2009).

5. CONCLUSIONS

Our ALMA Early Science observations of the molecular gas in the A1664 BCG reveal two massive molecular gas flows, each with a mass of $M_{\rm mol} \sim 5 \times 10^9\,M_\odot$. The component centered on the BCG systemic velocity shows a smooth velocity gradient across the BCG center from −250 to 250 km s^{-1} with velocity proportional to radius. Although this is suggestive of rotation about the nucleus, the mass and velocity structure are highly asymmetric and could indicate an inflow of gas in the process of forming a relaxed disk. The HVS consists of two gas clumps, each ∼2 kpc across at a velocity of −570 km s^{-1} with respect to the systemic velocity. Each clump has a velocity dispersion of ∼250–300 km s^{-1} and there is an increase in the velocity of the gas toward the nucleus from -510 ± 20 km s^{-1} to -590 ± 10 km s^{-1}. This velocity gradient could signify a high-velocity inflow onto the nucleus with the broad velocity shear indicating that the acceleration is along an axis close to the line of sight. However, the HVS is also coincident with regions of low optical–UV surface brightness, which could trace dust extinction associated with each clump. The high-velocity gas would then be a massive outflow projected in front of the BCG and moving toward us along the line of sight. Based on the energy requirements, we suggest that this outflow would most likely be driven by the central AGN. A merger origin for the HVS is possible but we consider it unlikely.

We thank the referee for helpful and constructive comments on the paper. H.R.R. and B.R.M. acknowledge generous financial support from the Canadian Space Agency Space Science Enhancement Program. R.A.M. and A.N.V. acknowledge support from the Natural Sciences and Engineering Research Council of Canada. A.C.E. acknowledges support from STFC grant ST/I001573/1. We thank the ALMA scientific support staff members Adam Leroy and Stéphane Leon. This paper makes use of the following ALMA data: ADS/JAO.ALMA#2011.0.00374.S. ALMA is a partnership of ESO (representing its member states), NSF (USA), and NINS (Japan), together with NRC (Canada) and NSC and ASIAA (Taiwan), in cooperation with the Republic of Chile. The Joint ALMA Observatory is operated by ESO, AUI/NRAO, and NAOJ. The National Radio Astronomy Observatory is a facility of the National Science Foundation operated under cooperative agreement by Associated Universities, Inc.

REFERENCES

Allen, S. W., Edge, A. C., Fabian, A. C., et al. 1992, MNRAS, 259, 67
Allen, S. W., Fabian, A. C., Edge, A. C., Bohringer, H., & White, D. A. 1995, MNRAS, 275, 741
Benson, A. J. 2005, MNRAS, 358, 551
Bîrzan, L., McNamara, B. R., Nulsen, P. E. J., Carilli, C. L., & Wise, M. W. 2008, ApJ, 686, 859
Bîrzan, L., Rafferty, D. A., McNamara, B. R., Wise, M. W., & Nulsen, P. E. J. 2004, ApJ, 607, 800
Bolatto, A. D., Wolfire, M., & Leroy, A. K. 2013, ARA&A, 51, 207
Burns, J. O. 1990, AJ, 99, 14
Combes, F., Young, L. M., & Bureau, M. 2007, MNRAS, 377, 1795
Condon, J. J., Cotton, W. D., Greisen, E. W., et al. 1998, AJ, 115, 1693
Cowie, L. L., Hu, E. M., Jenkins, E. B., & York, D. G. 1983, ApJ, 272, 29
Crawford, C. S., Allen, S. W., Ebeling, H., Edge, A. C., & Fabian, A. C. 1999, MNRAS, 306, 857
De Breuck, C., Tang, Y., de Bruyn, A. G., Röttgering, H., & van Breugel, W. 2002, A&A, 394, 59
Donahue, M., Jordán, A., Baum, S. A., et al. 2007, ApJ, 670, 231
Donahue, M., Mack, J., Voit, G. M., et al. 2000, ApJ, 545, 670
Draine, B. T., & Salpeter, E. E. 1979, ApJ, 231, 77
Dunn, R. J. H., & Fabian, A. C. 2006, MNRAS, 373, 959
Edge, A. C. 2001, MNRAS, 328, 762
Edge, A. C., & Frayer, D. T. 2003, ApJL, 594, L13
Egami, E., Misselt, K. A., Rieke, G. H., et al. 2006, ApJ, 647, 922
Ekers, R. D., & Simkin, S. M. 1983, ApJ, 265, 85
Emonts, B. H. C., Morganti, R., Tadhunter, C. N., et al. 2005, MNRAS, 362, 931
Fabian, A. C. 1994, ARA&A, 32, 277
Fabian, A. C., Johnstone, R. M., & Daines, S. J. 1994, MNRAS, 271, 737
Ferland, G. J., Fabian, A. C., Hatch, N. A., et al. 2009, MNRAS, 392, 1475
Ferland, G. J., Fabian, A. C., & Johnstone, R. M. 1994, MNRAS, 266, 399
Hamer, S. L., Edge, A. C., Swinbank, A. M., et al. 2014, MNRAS, 437, 862
Heckman, T. M. 1981, ApJL, 250, L59
Hernquist, L., & Springel, V. 2003, MNRAS, 341, 1253
Hu, E. M., Cowie, L. L., & Wang, Z. 1985, ApJS, 59, 447
Jablonka, P., Combes, F., Rines, K., Finn, R., & Welch, T. 2013, A&A, 557, 103
Johnstone, R. M., Fabian, A. C., & Nulsen, P. E. J. 1987, MNRAS, 224, 75
Kennicutt, R. C., Jr. 1998, ARA&A, 36, 189
Kirkpatrick, C. C., McNamara, B. R., Rafferty, D. A., et al. 2009, ApJ, 697, 867
Lim, J., Ao, Y., & Dinh-V-Trung. 2008, ApJ, 672, 252
Markwardt, C. B. 2009, in ASP Conf. Ser. 411, Astronomical Data Analysis Software and Systems XVIII, ed. D. A. Bohlender, D. Durand, & P. Dowler (San Francisco, CA: ASP), 251
McMullin, J. P., Waters, B., Schiebel, D., Young, W., & Golap, K. 2007, in ASP Conf. Ser. 376, Astronomical Data Analysis Software and Systems XVI, ed. R. A. Shaw, F. Hill, & D. J. Bell (San Francisco, CA: ASP), 127
McNamara, B. R., & Nulsen, P. E. J. 2007, ARA&A, 45, 117
McNamara, B. R., Russell, H. R., Nulsen, P. E. J., et al. 2013, ApJ, submitted (arXiv:1309.0013)
Mittal, R., O'Dea, C. P., Ferland, G., et al. 2011, MNRAS, 418, 2386
Morganti, R., Oosterloo, T., & Tsvetanov, Z. 1998, AJ, 115, 915
Morganti, R., Oosterloo, T. A., Tadhunter, C. N., et al. 2004, A&A, 424, 119
Morganti, R., Tadhunter, C. N., & Oosterloo, T. A. 2005, A&A, 444, L9
Nesvadba, N. P. H., Lehnert, M. D., Eisenhauer, F., et al. 2006, ApJ, 650, 693
O'Dea, C. P., Baum, S. A., Privon, G., et al. 2008, ApJ, 681, 1035
O'Dea, K. P., Quillen, A. C., O'Dea, C. P., et al. 2010, ApJ, 719, 1619
Oosterloo, T. A., Morganti, R., Tzioumis, A., et al. 2000, AJ, 119, 2085
Panagoulia, E. K., Fabian, A. C., & Sanders, J. S. 2013, MNRAS, 433, 3290
Peres, C. B., Fabian, A. C., Edge, A. C., et al. 1998, MNRAS, 298, 416
Peterson, J. R., & Fabian, A. C. 2006, PhR, 427, 1
Pimbblet, K. A., Smail, I., Edge, A. C., et al. 2006, MNRAS, 366, 645
Pope, E. C. D., Babul, A., Pavlovski, G., Bower, R. G., & Dotter, A. 2010, MNRAS, 406, 2023
Quillen, A. C., Zufelt, N., Park, J., et al. 2008, ApJS, 176, 39
Rafferty, D., McNamara, B., & Nulsen, P. 2008, ApJ, 687, 899
Revaz, Y., Combes, F., & Salomé, P. 2008, A&A, 477, L33
Salomé, P., & Combes, F. 2003, A&A, 412, 657
Salomé, P., Combes, F., Edge, A. C., et al. 2006, A&A, 454, 437
Salomé, P., Combes, F., Revaz, Y., et al. 2011, A&A, 531, A85
Salomé, P., Revaz, Y., Combes, F., et al. 2008, A&A, 483, 793
Simkin, S. M. 1979, ApJ, 234, 56

Solomon, P. M., Rivolo, A. R., Barrett, J., & Yahil, A. 1987, ApJ, 319, 730
Solomon, P. M., & Vanden Bout, P. A. 2005, ARA&A, 43, 677
Tadhunter, C. N. 1991, MNRAS, 251, 46P
Toomre, A. 1964, ApJ, 139, 1217
Veilleux, S., Cecil, G., & Bland-Hawthorn, J. 2005, ARA&A, 43, 769
Veilleux, S., Cecil, G., Bland-Hawthorn, J., & Shopbell, P. L. 2002, RMxAC, 13, 222
Voit, G. M., & Donahue, M. 1995, ApJ, 452, 164
Voit, G. M., & Donahue, M. 2011, ApJL, 738, L24
Vollmer, B., Braine, J., Pappalardo, C., & Hily-Blant, P. 2008, A&A, 491, 455
von der Linden, A., Best, P. N., Kauffmann, G., & White, S. D. M. 2007, MNRAS, 379, 867
Wagner, A. Y., Bicknell, G. V., & Umemura, M. 2012, ApJ, 757, 136
Wilman, R. J., Edge, A. C., & Johnstone, R. M. 2005, MNRAS, 359, 755
Wilman, R. J., Edge, A. C., & Swinbank, A. M. 2006, MNRAS, 371, 93
Wilman, R. J., Edge, A. C., & Swinbank, A. M. 2009, MNRAS, 395, 1355
Young, L. M., Bureau, M., Davis, T. A., et al. 2011, MNRAS, 414, 940